Tellus (1987), *39B*, 293–317

On radiative effects of anthropogenic aerosol components in Arctic haze and snow

By JEAN-PIERRE BLANCHET† and ROLAND LIST, *Department of Physics, University of Toronto, Canada, M5S 1A7*

(Manuscript received September 2, 1985; in final form July 31, 1986)

ABSTRACT

The Arctic aerosol is strongly enriched by anthropogenic pollution which may cause significant modifications of the Arctic climate. A radiation model with an optically interactive snow surface layer is developed to investigate the effect of anthropogenic elemental carbon (EC) and sulphuric acid in the Arctic atmosphere. The model, based on the delta-Eddington method, has 490 wavelength intervals covering solar and terrestrial radiation domains. Computations were made for aerosols-containing natural components and cases contaminated by anthropogenic EC and sulphuric acid, both categories with dry and moist conditions. Comparisons of model results with measurements in the Arctic of direct and total irradiance agree well. During mid-spring averaged conditions, the increase in the daily mean solar warming is found to be 2 or 3 times lower than earlier estimates. The previously expected surface cooling can be offset by direct to diffuse conversion in the haze and by snow contamination. In the infrared, the haze located in a temperature inversion can increase the upwelling irradiance by about 1%. This earth-atmosphere column cooling is caused by deliquescent aerosol material. In contrast, hygroscopic but non-deliquescent compounds like sulphuric acid result in internal exchange of radiative energy. In haze layers, the local cooling rate nearly offsets the daily averaged mid-spring local solar heating rate. More significant net warming due to EC particles takes place in dry and optically thin aerosol layers typically found above the Arctic boundary layer during pollution episodes.

1. Introduction

During the past few years, the existence of anthropogenic components in the Arctic aerosol has been clearly established (Rahn and McCaffrey, 1979; Heintzenberg, 1980, 1981). One of the persistent questions concerning any man-made perturbation to the atmosphere concerns its influence on climate. The Arctic is an important source region for the generation of available potential energy particularly during winter time. Furthermore, in the absence of solar forcing during winter the typical damping of the radiative perturbation due to short diurnal cycles, normally found at lower latitudes, does not apply to the Arctic. The continuous insolation during spring results in a long period of heating. A second consideration in understanding the effect of the Arctic aerosol is the enhancement of the solar heating due to the increased path length for absorption above the highly reflective snow surfaces in Polar regions.

Because of such considerations, measurements of physical and chemical characteristics of the Arctic aerosol have received considerable attention during the last decade. Representative models of the optical properties have been established (Patterson et al., 1982; Blanchet and List, 1983) and some measurements on radiative behaviour of the haze have been obtained (Mendonca et al., 1981; Valero et al., 1983). Other studies have investigated the effect of the aerosol on the solar

† Present affiliation: Canadian Climate Center City of North York, Ontario, Canada, M3H 5T4.

radiation budget (Shaw and Stamnes, 1980; Porch and McCraken, 1982; Cess, 1983). However, before attempting a climate study, it is necessary to acquire a detailed view of the radiative effects of the Arctic aerosol.

The present paper is an attempt to examine in detail the radiative effects of the main components of the aerosol. Using an aerosol model (Blanchet and List, 1983), spectral and integrated irradiances at the surface and at the top of the atmosphere are investigated from a narrow band radiation model where the perturbation amplitude of the thermal and solar radiation budget is the most direct effect of the arctic haze. However, this is poorly known at the moment and requires further investigation. Other unknown effects are those due to contamination of the snow surface and atmospheric moisture.

The usefulness of a diagnostic study of the radiation budget is two fold. First, it is necessary to gain detailed understanding of the physical processes involved. High-order climate models such as general circulation models (GCM) generally require simple but adequate parameterization for most physical processes. Second, the strength of the perturbation should be assessed before proceeding to detailed time dependent studies in order to determine which of the interactions are significant. The natural variability of the Arctic climate is very large and for all practical purposes a weak perturbation might just be statistically insignificant over a typical GCM simulation period.

The first estimation of the effect of the Arctic haze on the earth-atmosphere radiation budget by Shaw and Stamnes (1980) indicated that the presence of the haze layer (optical depth $\tau = 0.2$, single scattering albedo $\omega = 0.8$ and asymmetry factor $g = 0.75$) heats the atmosphere by 20 to 30 w m^{-2} and cools the surface by about 5 w m^{-2}. The calculations were made for monochromatic radiation at 0.5 μm. Accoring to Blanchet and List (1983) a single scattering albedo $\omega = 0.8$ is reasonable for dry aerosol while $\tau = 0.2$ is more representative of the haze layer close to saturation ($\omega - > 1$), thus leading to a rather large optical thickness for absorption. However their calculations showed clearly that the Arctic haze has a tendency to heat the atmosphere and cool the surface with a net gain for the earth-atmosphere column.

Porch and MacCracken (1982) used the detailed solar radiation model of Dave (1972) to perform a similar experiment. However they used a simple estimate of the dry aerosol optical properties by matching arbitrary size distributions and refractive index ($1.5–0.1i$) and by varying the particulate concentration (1480 cm^{-3}) to produce an effective absorption coefficient of 0.0045/km at 0.5 μm as observed by Rosen et al. (1981). This procedure led to an optical thickness for absorption of 0.038 at 0.55 μm and single scattering albedo of 0.45 for their "small" distribution. For a solar zenith angle of 72° and a surface albedo of 0.8, the aerosol layer produced a flux convergence of about 20 w m^{-2} in the atmosphere, in agreement with results of Shaw and Stamnes. In this case the optical properties are representative of the dry anthropogenic aerosol although the optical depth for absorption may be overestimated by more than a factor 2 due to the Laser Transmission Method used to determine the absorption coefficient (Sadler et al., 1981). By accounting for the diurnal cycle during mid-spring the atmospheric heating due to aerosol is reduced to about 5 w m^{-2}.

More recently, Cess (1983) performed a series of experiments using a simple parameterized two layer solar radiation model of the atmosphere. The main results were the following: (1) the vertical distribution of aerosols has little effect upon the earth-atmosphere radiation budget, (2) due to the high surface albedo, scattering by the aerosol has only a minor effect on the earth-atmosphere radiation budget, (3) the earth-atmosphere radiation balance is insensitive to the relative humidity, within the range of 70 to 95% despite a large change in the aerosol optical depth, (4) the surface radiation balance is decreased due to reduced incident solar radiation at the surface from aerosol absorption and scattering, (5) the presence of background natural aerosol has little effect on anthropogenic and total aerosol perturbations of the system radiation balance. However this study does not account for snow albedo interaction nor the high relative humidities (RH > 99%) characteristic of haze episodes, both of which might alter the net result.

In previous studies the atmospheric thermal radiation was omitted due to the uncertainties in modelling the problem and the expectation of

negligible effects on the basis of low infrared aerosol opacity (Shaw and Stamnes, 1980). Porch and MacCracken recognized the need for investigation of the aerosol effect in the infrared regime along with snow-aerosol and cloud-aerosol interactions. As shown by Blanchet and List (1983), the dry aerosol has a low infrared opacity for extinction, approximately 50 times smaller than the opacity in the mid-visible. However, at relative humidities typically close to saturation for haze episodes, and due to the large amount of water collected by the aerosol, the absorption coefficient increases rapidly at infrared wavelengths and largely surpasses the mid-visible absorption coefficient.

So far, radiation budget studies have overlooked the optical properties of the snow surface by assuming a fixed lambertian reflectivity. In fact a snow layer may be seen as a thick aerosol layer composed of large ice grains and confined to the bottom of the atmosphere. Such a layer interacts with the above atmosphere in several ways. The ratio of diffuse to direct radiation as altered by the haze, changes the albedo. The changes in absorption by atmospheric constituents also affect the albedo. Multiple scattering between snow and the haze layer or clouds are known to be important for absorption at visible wavelengths (Wiscombe, 1973) and is strongly wavelength dependent. Finally the deposition of aerosol material on the surface is likely to affect the radiation budget principally during snow melt where dust-like material tends to accumulate on the surface. Although included in the present model these effects will be more thoroughly discussed in a separate paper.

Studies on the effect of aerosol on the radiation budget at lower latitudes demonstrate the competing action between reflected solar energy and emitted thermal energy. The net energetic effect of an aerosol may be small as is expected in the case for Sahara dust blown over eastern Atlantic (Carlson and Benjamin, 1980). However in polar regions the situation differs due to the long diurnal cycle and the considerable decoupling between solar and thermal domination. The winter season is essentially a long period of nocturnal cooling while late spring is characterized by maximum incident solar radiation on the globe due to continuous sunshine. Further, the long atmospheric paths and the large surface albedo greatly enhance the effect of aerosols at high latitude. As a result even a modest aerosol amount may have a significant effect.

Visual observation of the Arctic haze from airplanes clearly shows the multi layer nature of the haze (Valero et al., 1983; Carlson, 1981). The variation of temperature and moisture profiles in conjunction with aerosol layers are likely to induce internal radiative energy exchange and damping of earth-atmosphere radiation perturbation particularly in the thermal regime.

Another particularity of the Arctic is the thermal structure of the atmosphere during winter when an anticyclonic regime prevails. The ground emits almost like a black body without receiving as much counter radiation from the atmosphere. Consequently the surface temperature is driven to a low equilibrium point. Meridional heat advection and air subsidence provides heat aloft and normally leads to strong temperature inversions. The energy lost by the surface is limited by its low temperature and poor thermal conductivity. On the other hand, haze and cloud layers located in this thermal inversion can potentially enhance the loss of radiative energy and provide a significant mechanism to affect the local climate. Furthermore, since most of the Arctic aerosol and particularly its anthropogenic constituents originate from low latitude source regions by eddy transport, the aerosol material is injected together with warm air and moisture. Consequently one might expect a related increase of the atmospheric opacity and cooling rate of the warm air in the Arctic.

The above considerations caused the reevaluation of the radiative properties of the Arctic haze by including the more detailed wavelength dependency of the aerosol model (Blanchet and List, 1983) and the snow model (Wiscombe and Warren, 1980). Calculations are extended to include thermal radiation. The effect of aerosol components are determined by their gradual removal. Cases for dry and hazy conditions are examined to determine the effect of moisture on the radiative perturbation.

2. The model

The radiation model is developed to account for anisotropic scattering due to cloud droplets

and aerosol particles. It is sufficiently general to treat any part of the radiation spectrum without discontinuity between the solar and terrestrial regimes. The eventual application to climate studies constrains on the mathematical formulation, to warrant computational efficiency coupled with a high degree of reliability. The applied delta-Eddington method (Joseph et al., 1977) is accurate to about 1% with respect to so called exact methods (Lenoble, 1976) for the range of conditions normally encountered in the troposphere. The development essentially follows that of Joseph et al. but includes the thermal source term.

Formally the radiative transfer equation (RTE) is

$$\mu \frac{dI}{d\tau} = -I + \frac{\omega}{4\pi} \int_0^{2\pi} \int_{-1}^{1} P(\mu,\phi;\mu',\phi') \times I d\mu' d\phi' + (1-\omega)\, B(T), \quad (1)$$

where $I = I(\tau, \mu, \phi)$ is the spectral radiance, μ is the cosine of the solar zenith angle θ, ϕ the azimuth, τ the optical depth, ω the single scattering albedo, P the scattering phase function and $B(T)$ the Planck function representing the isotropic thermal source at temperature T.

The delta-Eddington method leads to rescaling the principal optical parameters, τ, ω and the asymmetry factor g, by the similarity relations such that the Eddington approximation of (1) remains in its most accurate range (Wiscombe and Joseph, 1977):

$$\tau' = (1-\omega g^2)\,\tau$$

$$\omega' = \frac{(1-g^2)}{(1-\omega g^2)}\,\omega \quad (2)$$

$$g' = \frac{g}{(1+g)}.$$

Upon applying transformations (2) to τ, ω and g, and substituting $I(\tau,\mu) = I_0(\tau) + I_1(\tau)\mu$ in (1) the RTE becomes identical to the well-known Eddington equation (*cf.* Shettle and Weinman (1970) and Wiscombe (1977)). After separation of the direct and diffuse components, (1) is further decomposed into upward ($\mu < 0$) and downward ($\mu > 0$) components leading to a pair of linear equations of the form

$$\frac{dG}{d\tau'} + \frac{3}{2}(1-\omega' g')H = \frac{3}{4}\omega' g' \mu_0 S \times \exp(-\tau'/\mu_0),$$

$$\frac{dH}{d\tau'} + 2(1-\omega')G = \frac{1}{2}\omega' S \times \exp\left(-\frac{\tau'}{\mu_0}\right) + 2\pi(1-\omega')B, \quad (3)$$

where S is the solar constant, $G = \pi I_0$ and $H = (2/3)\pi I_1$ with I_0 and I_1 as diffused components. The solution in each homogeneous layer is

$$G = C_1 \exp(\lambda\tau') + C_2 \exp(-\lambda\tau') - \bar{\alpha} \times \exp\left(\frac{-\tau'}{\mu_0}\right) + B,$$

$$H = -C_1 \boldsymbol{P} \exp(\lambda\tau') + C_2 \boldsymbol{P} \exp(-\lambda\tau') - \bar{\beta} \times \exp\left(\frac{-\tau'}{\mu_0}\right) - \frac{\boldsymbol{P}}{\lambda}\frac{dB}{d\tau'} \quad (4)$$

where

$$\lambda = \sqrt{3(1-\omega')(1-\omega' g')},$$

$$\boldsymbol{P} = \frac{2}{3}\frac{\lambda}{(1-\omega' g')},$$

$$\bar{\alpha} = \frac{3}{4}\omega' S \frac{1+g'(1-\omega')}{(1/\mu_0)^2 - \lambda^2},$$

$$\bar{\beta} = \frac{1}{2}\omega' S \frac{3g'(1-\omega')\mu_0 + (1/\mu_0)}{(1/\mu_0)^2 - \lambda^2}$$

$$\frac{dB}{d\tau'} = \text{constant} = \frac{\Delta B}{\Delta\tau'}.$$

Finally the upward and downward fluxes are given by

$$F^{\uparrow} = G - H,$$

$$F^{\downarrow} = G + H + \mu_0 S \exp\left(\frac{-\tau'}{\mu_0}\right), \quad (5)$$

and the radiative heating rate by

$$\frac{dT}{dt} = \frac{-g_0}{C_p}\frac{d}{dp}(F^{\downarrow} - F^{\uparrow}), \quad (6)$$

where g_0 is the acceleration due to gravity, C_p is the specific heat at constant pressure and p is the pressure.

In the model, the atmosphere is represented by

n homogeneous layers, linked by continuity equations in upward and downward irradiances. Two more boundary conditions are required. At the top of the model, the incident solar flux is depleted by absorption of the direct solar radiation by gases neglecting any scattering. The atmospheric thermal emission above the highest model level is approximated by narrow band grey emission of a single layer containing the remaining gases above that level. At the surface or at the snow-ground interface (when snow is present), the spectral albedo imposes the usual lower boundary condition

$$(1-A)G_{n-1}(\tau_n') - (1+A)H_{n-1}(\tau_n') = F_0^{\downarrow} + A\mu_0 S \times \exp\left(\frac{-\tau_n'}{\mu_0}\right). \quad (7)$$

The remaining difficulty concerns the evaluation of the optical depth for gaseous absorption $\tau(g)$. For monochromatic radiation, the transmission through a layer of gas amount u and absorption coefficient $K(\lambda)$ is given by

$$\mathrm{Tr}_\nu = \exp(-\tau_\nu), \quad (8)$$

where $\nu = \lambda^{-1}$, λ is the wavelength and

$$\tau_\nu = \int k_\nu \, du,$$

leading to the so-called "line-by-line" calculation which is prohibitive in computer time, because of the large variation of k. To avoid this difficulty the usual procedure is to express the transmission over finite spectral regions $\Delta\nu$ by a series of the form

$$\mathrm{Tr} = \sum_k p_k \exp(-c_k U) \quad (9)$$

where p_k is a statistical weight ($\sum p_k = 1$) and c_k is an absorption coefficient. Generally 5 to 10 terms are necessary to reach accuracy of about 1% of transmission. This method known as the "exponential sum fitting for the transmission" (ESFT) has two inconveniences. The first one concerns the pressure and temperature dependence of c_k. It is usual to employ an empirical scaling on gas amount of the form

$$u^* = u\left(\frac{p}{p_0}\right)^n \left(\frac{T_0}{T}\right)^m, \quad (10)$$

where p and T are respectively the pressure and the temperature at a given height and p_0 and T_0 the corresponding reference values (laboratory conditions). For very large u (strong line approximation), $\eta = 1$, while for small u (weak line approximation) $\eta = 0$. In practice, a typical spectral interval is composed of a mixture of weak and strong lines that (for further complications) may overlap. It is therefore expected that η ranges somewhere between 0 and 1. The value of η is generally supported by experimental measurements (McClatchey et al., 1973). Typically, $\eta = 0.90$, 0.40 and 0.75 for water vapour, ozone and uniformly mixed gases, respectively. On the other hand, the temperature scaling ($(T_0/T)^m$) is not well justified. It is known that the temperature dependence of the absorption coefficient is significant particularly in the terrestrial regime and that it varies considerably with wavelength.

The second inconvenience arises from the treatment of band overlap. Using the product of the transmissivity for each gas, (9) leads to k^2 terms for 2 gases and k^3 terms for three gases. The number of sub-intervals may easily reach several thousands; increasing the work load proportionally.

A different approach is examined as an alternative to ESFT. Noting that the RTE only requires the optical depth, the single scattering albedo and the asymmetry factor as input parameters and that the random band model (Goody or Malkmus models) for transmission in gaseous layers takes a form analogous to (8)

$$\mathrm{Tr} = \exp\left(\frac{-\sum W_i}{\Delta\nu}\right), \quad (11)$$

where $\sum W_i$ is the sum of equivalent width of individual lines and $\Delta\nu$ is the wave number interval width. An effective optical depth can be defined as

$$\tau_e = \frac{\sum W_i}{\Delta\nu}, \quad (12)$$

In particular, for the Malkmus band model:

$$\tau_e = \frac{c_2}{2}\left(\sqrt{1 + 4u\,(c_1/c_2)} - 1\right) \quad (13)$$

where c_1 and c_2 are band parameters. τ is not any more a linear function of the gas amount and, unlike (8), is not additive over consecutive layers. However, apart from the treatment of the direct solar beam, the scattering problem (3) considers only individual layers. This method requires only

one RTE calculation per wave number interval and accounts for the temperature dependency in a consistent manner. Following Rodgers and Walshaw (1966), one can define

$$c_1 = \frac{k}{d}\Phi(T)$$

$$c_2 = \frac{\pi\alpha_0}{d}\frac{\Phi(T)}{\psi(T)}\frac{p}{p_0}, \tag{14}$$

where α_0 is the mean half-width, k the mean line strength, d the mean line spacing, p_0 the reference pressure and

$$\Phi(T) = \exp(a(T-260) + b(T-260)^2)$$

$$\psi(T) = \exp(a'(T-260) + b'(T-260)^2) \tag{15}$$

where coefficients a, b, a', b' are evaluated from band parameters at three distinct temperatures (220, 260 and 300°K). For the pressure dependency, the Curtis-Godson approximation for homogeneous layers becomes simply the mean pressure $p = (p_i + p_{i+1})/2$.

In the solar regime, for a clear atmosphere, the direct beam dominates (typically 80% of the total down flux at the surface) and the transmittance must be calculated using the cumulative gas amount between the top of the model and the reference level. Then the optical depth of individual layers is approximated by the finite difference of the optical depth for the direct beam. Even though (13) is not additive, this approximation is correct for the direct beam and acceptable for the weaker diffuse component ($\approx$20% of the total at the surface). This assumption was verified by executing the model, for conditions used in this study, with the ESFT method for transmission in gases and comparing the results to those from the band model approximation. It was found that the total transmission of the downward flux between the top and the surface is lower by 1.7% in the case of the band model approximation. Because of the long path, the Curtis-Godson approximation is used to find an effective pressure for that path z

$$\bar{p} = \frac{\int p u dz}{\int u dz}. \tag{16}$$

In a similar way, a mean temperature for that path is given by

$$\bar{T} = \frac{\int T u dz}{\int u dz}. \tag{17}$$

Band parameters k/d and $\pi\alpha_0/d$ for gases are obtained by summing parameters for individual lines

$$\frac{k}{d} = \frac{\sum k_i}{\Delta\nu},$$

$$\frac{\pi\alpha_0}{d} = \frac{4\pi}{\Delta\nu}\frac{(\sum\sqrt{k_i\alpha_i})^2}{\sum k_i}. \tag{18}$$

AFGL spectral data (Rothman, 1981) are used. About 159,000 rotational and vibration-rotation transitions for 7 gases (water vapour, carbon dioxide, ozone, nitrous oxide, carbon monoxide, methane and molecular oxygen) are considered between 0.56 and 33,300 μm. At shorter wavelengths, in the UV and in the visible, molecular oxygen and ozone are treated by a single parameter approximation, i.e. the optical depth is simply ku. The molecular scattering coefficient is given by Edlen's equation

$$(n_a - 1) = \left[64.328 + \frac{29498.1}{(146 - 1/\lambda^2)} + \frac{255}{(41 - 1/\lambda^2)}\right] \times 10^{-6},$$

$$\beta_{sc} = \frac{8\pi^3}{3}\frac{(n_a^2-1)^2}{\lambda^4 N_0}\frac{P}{P_0}\frac{T_0}{T}\left(\frac{6+3\rho_n}{6-7\rho_n}\right), \tag{19}$$

where N_0 is the number of molecules, ρ_n the depolarization factor and λ the wavelength. Further the attenuation coefficient for the water vapour continuum has been included (Roberts et al., 1976),

$$\tau(c) = Cu(H_2O)\left[\frac{p_h}{p_0}\exp\left\{6.08\left(\frac{296}{T} - 1\right)\right\} + 0.002 \times \left(\frac{p - p_h}{p_0}\right)\right], \tag{20}$$

where p_h is the partial pressure of water vapour and $C(g^{-1}\,cm^{-2}\,atm^{-1})$ in the 8 to 14 μm region is given by

$$C(\nu, T) = C(\nu, 296°K)\exp\left[1800\left(\frac{1}{T} - \frac{1}{296}\right)\right], \tag{21}$$

$$C(\nu,296) = 4.18 + 5578 \exp\{-0.0787\ \nu(\mathrm{cm}^{-1})\},$$

and in the 3 to 4 μm by

$$C(\nu,296°\mathrm{K}) = 0.1058 - 4.16 \times 10^{-5} \times (\nu - 2600\ \mathrm{cm}^{-1}) + 1.57 \times 10^{-6} \times (\nu - 2600)^2. \quad (22)$$

Finally the total optical depth is the sum of contributions by gaseous absorption, continuum, aerosol, clouds, snow and molecular scattering:

$$\tau = \sum \tau_i. \quad (23)$$

Similarly, the total single scattering albedo and asymmetry factor are given by

$$\omega = \frac{\sum \tau_{sc_i}}{\tau}, \qquad g = \frac{\sum \tau_{sc_i} g_i}{\sum \tau_{sc_i}}. \quad (24)$$

The solar spectrum fully overlaps with the terrestrial regime in the infrared up to 50 μm. Data for the solar irradiance are interpolated from Thekaekara (1974). A daily mean solar zenith angle and insolation period are found from (Cogley and Borucki, 1976):

$$\mu_0 = \frac{U}{2T'}, \quad (25)$$

$$U = 2\left\{A^2 T' + 2\frac{AB}{\omega_0}\sin(\omega_0 T') + \frac{B^2}{4\omega_0}\sin(2\omega_0 T') + \frac{B^2 T'}{2}\right\}$$

$$T' = \frac{1}{\omega_0}\cos^{-1}\left(\frac{-A}{B}\right) \qquad A = \sin L \sin D \qquad B = \cos L \cos D$$

where L and D are the latitude and the solar declination, ω_0 is the angular velocity of the earth's rotation and T' is the half-day length and is bounded by 0 and 12 h. In the model the solar declination is approximated by a 7-term Fourier expansion.

The snow cover is treated in a similar manner as the aerosol. In the present model, the procedure used by Wiscombe and Warren (1980) has been generalized to a multi-layer snow cover with direct coupling to atmospheric radiation by treating each snow layer as part of atmospheric layers. At the bottom of the model, ten layers were reserved for snow cover at the ground. The optical parameters for snow grain were those published by Wiscombe and Warren (1980). Because of the thin geometric depth and thick optical depth of snow layers, the absorption by gases are neglected in those layers. However aerosol material similar to that found in the haze may be added to snow in order to investigate the effect of aerosol deposition on the radiation balance.

2.1. Accuracy of the model

The accuracy of the delta-Eddington approximation has been thoroughly tested (Joseph et al., 1976; Wiscombe and Joseph, 1977; Lenoble, 1976; Welch and Zdunkowski, 1982). Wiscombe and Joseph (1977) demonstrated by extensive tests that when the phase function has only a weak forward peak ($g < 0.5$, i.e. $g < 1$ for the delta-Eddington approximation), the conventional Eddington approximation is typically 1% accurate outside some specific problem areas. A maximum absolute error of nearly 5% occurs at intermediate optical depth ($\tau \approx 1$) and mid-range of single scattering albedo ($\omega \approx 0.5$). These authors also point out that the results are weakly dependent on the details of the phase function. In the present model, the optical thickness of layers is typically small in the visible ($\tau \approx 0.001$) and very large in the infrared ($\tau \approx 100$), further the occurrence of mid-range optical depths is in most cases only transitory. Joseph and Wiscombe (1976) showed that the average relative error of the delta-Eddington approximation over wavelength, diurnal course and geographical location is approximately 0.3%. All comparisons were made against an exact method, the adding and doubling scheme (Hansen, 1969).

The main limitation of the radiation model is not in the method used to solve the RTE but rather in the approximation employed to evaluate the transmission function in the gaseous atmosphere. The basic line parameters obtained from laboratory measurements typically have an accuracy of the order of 10% (Kneizys et al., 1980). In the calculation those parameters were further averaged over a large number (≈ 300) of lines in each spectral interval by means of the Malkmus band model. Band models typically have a minimum accuracy in the medium range of transmittance (0.5) which is also transitory. But in the following experiments, errors associated

with gaseous transmission are systematic errors. All their effects are practically eliminated when a sensitivity experiment is performed, i.e., when the deviation due to a small perturbation is examined, particularly if that perturbation, like grey absorption and scattering due to aerosols, only weakly interacts with gas absorption. In practical terms, this means that the magnitude of fluxes and total heating rates are accurate to approximately 10% while deviation due to aerosol perturbations are limited to the accuracy of the aerosol optical parameters to within a few percent.

To verify the accuracy of the radiation model, the computer code is executed for prescribed conditions that are identical to those from results of independent studies. LOTRAN 5 (Kneizy et al., 1980) is a recent version of a code developed by the Air Force Cambridge Research Laboratory (AFCRL) and was designed to compute transmittance and thermal radiance over given atmospheric paths. The geometry is slightly different since LOTRAN 5 accounts for the curvature of the atmosphere while the present radiation model assumes a plane parallel atmosphere. On the other hand LOTRAN 5 ignores multiple-scattering. LOTRAN has been compared with observations (Kneizys et al., 1980) and was shown to be reliable for low transmission and emission spectra. In Fig. 1 the thermal radiance computed by the present radiation model is compared to that of LOTRAN 5 for a standard tropical atmosphere (McClatchey et al., 1973). The solid dots represent the downward radiance at the surface level from an effective zenith angle of 53°. The main discrepancy occurs in the window near wave number 1200 cm^{-1} and is due to larger optical depth from the approximation (13). The open dots show the radiance emerging at the top of the model for the same zenith angle of 53°. Overall, the agreement between the two models is remarkable. The most significant error is obtained in the downward component at the surface in the window near 1200 cm^{-1} where the band model in (13) overestimates the optical depth. Further test calculations (Luther and Fouquart, 1984) on standard atmosphere showed that this localized error is in the range of 5 to 10% and is due to the water vapour band model in the mid range of transmittance.

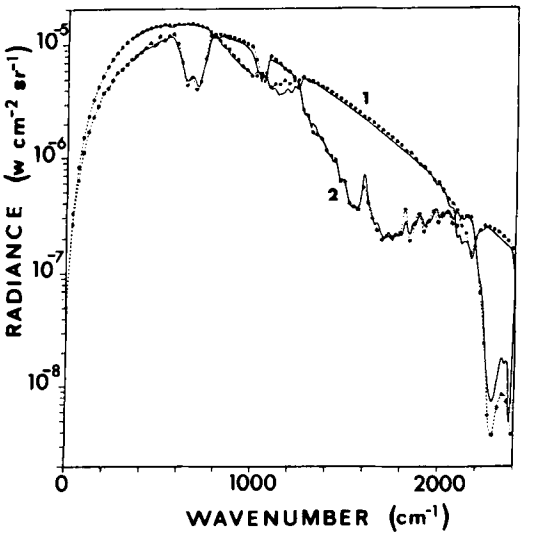

Fig. 1. Comparison of the thermal radiance from the radiation model (dots and dashed lines) to that of LOTRAN 5 (solid lines). The solid dots (1) are for the downward component received by the surface while the open dots (2) represent the upwelling radiance at the top. In both cases the standard tropical atmosphere (McClatchey et al., 1974) is used.

Fig. 2 illustrates the accuracy of the radiation model to compute the transmittance of the direct solar beam along a slanted path ($\theta = 53°$) between the top and the surface of the standard tropical atmosphere. The solid line was obtained from LOTRAN 5 for the same conditions. The visible region (0.3 to 0.7 μm) is dominated by molecular scattering. Weak absorption bands for wavelengths smaller than 0.69 μm are not included in LOTRAN 5. Thus, on occasions (near 0.6 and 0.7 μm) the transmittance differs significantly from the band model used in LOTRAN. Similar comparisons for the infrared spectrum are shown in Fig. 2.

Radiation models are sensitive to errors in flux divergence. Fig. 3 shows a comparison of the model with the results from an improved version of the scheme from Rodgers and Walshaw (1966) in a test standard atmosphere proposed by Stone and Manabe (1968). The larger cooling below 800 mb is due to the collison broadening and the dimer contribution in the water vapour window region. This effect was ignored in the scheme of Rodgers and Walshaw but essentially agrees with the study by Grassl (1972). Although not shown

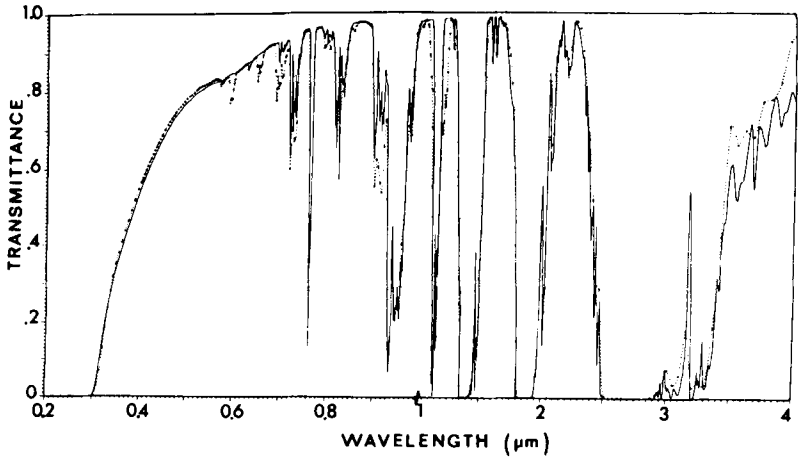

Fig. 2. Solar transmittance between the top and the surface of the model (--+--+--) for the visible and IR regions as compared to similar results from LOTRAN 5 (solid line). The same tropical atmosphere with a solar zenith angle of 53° was used in both cases.

in Fig. 3, the results from the model underestimates the infrared cooling in the upper atmosphere (above 10 mb). This error becomes particularly significant around 1 mb. In that region, the Doppler broadening is important and the Voigt line profile needs to be considered for a proper treatment. However, because of the small amount of gaseous absorbers, the influence of the upper atmosphere on the radiation balance is small and may be neglected for lower atmosphere problems.

In conclusion, the radiation model presented appears accurate and reliable for investigating the Arctic haze.

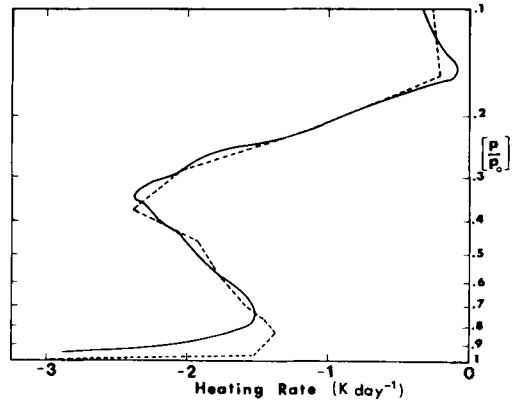

Fig. 3. Comparison of the radiative heating rate from the model (wavelengths > 4 μm) (solid line, with continuum) to that computed by Stone and Manabe (1968) (dashed line) using the model of Rodgers and Walshaw (1966) for the same tropical atmosphere (without continuum).

3. Experiment

The first objective of the experiment is to examine the effect of the main anthropogenic aerosol components (soot or elemental carbon (EC), sulphuric acid and remaining material) on the radiative perturbation at the surface and at the top of the model. Secondly the vertical and spectral perturbations of the radiation field are investigated.

The optical properties of the aerosol are those given by Blanchet and List (1983). Three aerosol models were set up to investigate the effect of EC and sulphuric acid which are considered to be the dominant anthropogenic substances in the Arctic aerosol. Model 3 is composed mostly of natural components; those are: soluble materials (69%), soil (18%) and sea salt (13%). A significant fraction of the soluble component is considered to be ammonium sulphate of anthropogenic origin. Model 3 is not a completely natural aerosol but has properties comparable to the cleanest aerosol observed in the Arctic during winter and spring.

This model is thereafter referred to as "basic aerosol". Model 2 has 0.4 $\mu g \cdot m^{-3}$ of EC in addition to the components of model 3. Finally model 1 is intended to represent a typically observed aerosol with anthropogenic components similar to those observed at Point Barrow Alaska during winter and spring. Its composition is approximately: 70% (by mass) of "basic aerosol" material, 24% of sulphuric acid and 6% of EC. In model 1 sulphuric acid is added to the composition of model 2.

The aim is not to do an extensive evaluation in a broad range of Arctic atmosphere conditions but rather to examine some typical situations. A few cases are selected to represent winter and spring for dry and moist conditions (Fig. 4). The winter case is selected for the thermal contrast between radiating surface and aerosol layer. For haze and no-haze conditions the criterion used by Mendonca et al. (1981) are adopted, that is a relative humidity of about 50% in no-haze and more than 99% in haze cases respectively. Some extreme conditions are also set to estimate the maximum potential perturbation.

The winter case was measured at Eureka North-West Territories, Canada on January 27 1957 (Rodgers and Walshaw, 1966). This profile is influenced by atmospheric subsidence as indicated by the maximum temperature and the minimum relative humidity near 1.8 km above the ground. The contrast between the surface temperature and the maximum at 1.8 km is more than 30°K. This is a typical sounding profile for the Arctic winter atmosphere under an anticyclonic regime. Such conditions are favorable for haze formation. The haze event is simulated by increasing the relative humidity (rh) to 99% in a layer of 0.6 km thickness within the thermal inversion (curve 2 in Fig. 4b). The associated aerosol profile is similar to that measured by Rahn (1978) at Barrow (Blanchet and List, 1983).

The case for spring condition was reported by Shaw (1975) during a haze episode on April 8, 1972 at Barrow, Alaska. The humidity profile was not measured by Shaw, however, the observed ice crystals precipitation is indicative of layers with relative humidities close to saturation. Three different profiles of relative humidity were assumed. The dryer profile (curve 3) as 50% rh at the ground corresponding to the no-haze condition. The second profile (4) has a moist layer, 0.3 km thick with 99.5% rh near the ground to repesent an average haze condition. Finally the extreme case (5) has a thick 1 km moist layer at 99.9% rh and is rather an upper limit for the haze. The aerosol density profile assumes a scale height of 1.5 km as observed by Shaw on that particular day. Shaw estimated the optical depth of the total aerosol column to 0.39 at 0.5 μm. The model produced optical depths of 0.081, 0.39 and 0.84 at 0.55 μm for each relative humidity profile (3, 4 and 5) respectively.

3.1. Comparisons of model results to observations and previous models

Comparisons of the model with observations permit us to assess the model and may help to interpret observations. Mendonca, DeLuisi and Schroder (1981) studied the radiation flux on

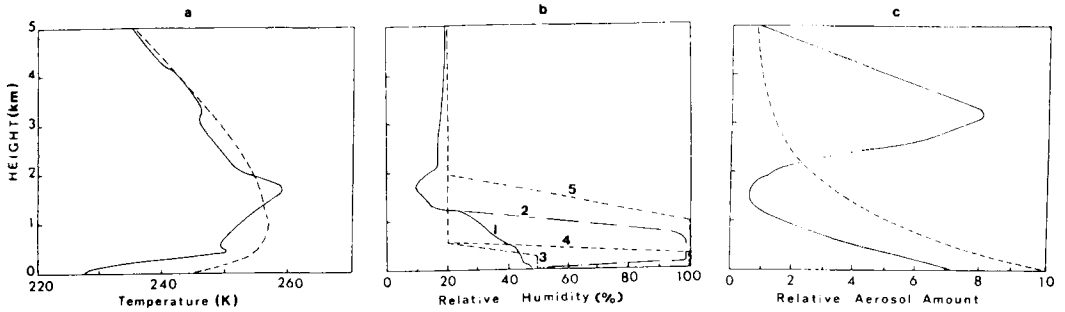

Fig. 4. Atmospheric conditions used in the present study. Temperature, relative humidity and aerosol concentration are shown for the lowest 5 km of the atmosphere. To convert aerosol amount to $\mu g \cdot m^{-3}$ the relative amount must be scaled by 1.31, 0.98 and 0.91 for dry aerosol model 1, 2 and 3, respectively. The dashed lines correspond to the spring case while the solid lines represent the winter case. Further details are given in the text.

cloudless days at the NOAA GMCC observatory located at Barrow, Alaska. Their results represent mean conditions for days during haze episodes and days with no visual haze. The results for broad band measurements (0.28 to 3.0 μm) are shown in Table 1 together with the present model results in the same spectral range. Their study shows an average depletion of 20% in the direct solar beam but only a depletion of 4.3% in the total downward flux, indicating strong conversion from direct to diffuse radiation. The depletion in total down flux is indicative of the change in absorption between haze and no haze conditions. This change is mostly due to the variations in atmospheric water vapour and water condensed on the aerosol as well as to possible changes in the dry aerosol material.

Conditions used in the model are more or less similar to those from observations and therefore, comparisons can be made. The case without aerosol showed only small and approximately equal changes in direct and diffuse solar fluxes. This result shows the weak sensitivity of the change in flux due to water vapour amount. In the case containing "basic aerosol" (model 3) scattering and absorption increased, but insufficiently to explain observations. Finally the case with added EC and sulphuric acid (model 1) is in close agreement with average observed haze. This indicates the necessity for a highly hygroscopic substance in the haze (such as sulphuric acid) accompanying the increase in EC in order to explain observations.

A comparison of the present model to the results from previous studies is shown in Table 2. Since previous studies considered mostly dry aerosol, the spring conditions without haze (50% rh at the ground) are used. Conditions are progressively degraded to show the effect of various assumptions in models. In previous studies the amplitude of the aerosol effect is estimated to more than 20 and -4 W m^{-2} for the change in the net solar irradiance at the top and at the surface respectively. The present cases resulted in lower effects with 6 to 8 W m^{-2} of total warming for the system and a slight surface warming for contaminated snow or slight cooling for pure snow. Besides the snow contamination, most of the differences are due to lower optical depths for absorption in the visible, the use of diurnal averages, and the direct to diffuse conversion on a non-Lambertian snow surface. Fixing the surface albedo to 78.12%, the zenith angle to 70.2° and increasing the optical depth for absorption to 0.0214 leads to results similar to those reported in previous studies. Further differences are due to slight discrepancies in conditions and methods used. The results from this model are consistent with observations as well as with other model studies.

Table 1. *Comparisons of conditions and changes in direct and diffuse irradiances at the ground between observations by Mendonca et al. (1981) and results from the model for cases examined in experiment 1*

	None (B0–A0)	Basic (B3–A3)	Anthropogenic (B1–A1)	M.D.S. (observed)
Humidity (%)				
no haze	50	50	50	55
haze	99	99.5	99.5	>99
Thickness (km)	0.41	0.3	0.3	<1
Zenith angle (degrees)	70.2	70.2	70.2	66.6
Optical thickness (0.5 μm)				
no haze	0.0	0.038	0.081	0.094
haze	0.0	0.17	0.39	0.21
Change in flux (%)				
direct beam	−1.2	−9.3	−18.8	−20.0
direct + diffuse	−1.0	−2.5	−4.7	−4.3

Indices A and B refer to dry and haze cases respectively while subindices 0, 1 and 3 refer to cases without aerosol, with aerosol model 1 and aerosol model 3 respectively. Further details are given in Table 4. The observed optical thickness (evaluated from direct beam) is lower than model values (total layer optical thickness) due to the omission of strong forward scattering in observed haze cases.

Table 2. *Changes in the solar radiation budget due to Arctic aerosol. Comparisons of the effect of the aerosol on net solar radiation at the top and the surface from previous studies with the no haze condition, with contaminated and pure snow; optical depths are given at 0.5 μm*

Studies	Optical depth for absorption	Change in net solar flux ($W \cdot m^{-2}$)	
Present study:		Top	Surface
(A1–A0) (contaminated snow)	0.012	7.76	+0.81
(A2–A0) (pure snow)	0.012	6.13	−0.92
(A2–A0) (fixed albedo = 78.12%)	0.012	7.37	−2.23
(A2–A0) (noon sun angle = 70.2°)	0.012	11.30	−3.42
(A2–A0) (optical depth)	0.0214	20.2	−6.1
Previous studies:			
Shaw and Stamnes (1980)	0.04	20 to 30	−4.7 to −6.2
Porch and MacCracken (1982)	0.0214	20.8	−4.1
Cess (1984)	0.0214	21.4	−4.7

4. Results and discussion

4.1. Radiation balance at the ground and at the top of the atmosphere

In the first experiment the atmospheric conditions are those observed by Shaw (1975) during a haze episode and referred above as "spring conditions". The solar declination for April 15 results in a daily mean zenith angle of 70.19° and a day fraction of 0.652 or 15.6 h of insolation. This results in an incident flux at the top of the atmosphere of 303.4 W m^{-2} representative of a daily average insolation during mid April at a latitude of 70°N. Cases (1) without aerosol, (2) with "observed aerosol", (3) with "observed aerosol" but pure snow and (4) with "basic aerosol" are performed for each relative humidity profile (3, 4 and 5 of Fig. 4b).

The main results are summarized in Table 3 in the form of net thermal ($\lambda > 3$ μm) and net solar ($\lambda < 3$ μm) fluxes at the top and surface of the model. The key to the labels describing the conditions are given in Table 4. The net flux is the difference between downward and upward fluxes at a particular reference level and represents the radiative energy gain (>0) or loss (<0) in the spectral region for the part of the atmosphere or snow below the reference level. The top of the model is set at 10 mb and the energy involved in the 1% of atmospheric mass above that level is neglected since it only weakly interacts with the haze. However depletion of the direct incident solar beam, mostly due to ozone, is accounted for up to pressure zero.

The same changes in conditions also apply to the aerosol material deposited in the snow layers. The influence of the contaminated snow is elaborated in a separate paper but some details must be introduced here. The snow on the ground is modelled by 10 layers of 1 cm of equivalent liquid water (ELW) and is, from the radiation point of view, nearly equivalent to a semi-infinite layer of snow (Wiscombe and Warren, 1980). An effective scavenging ratio of 102,000 is applied to account for all forms of wet and dry deposition processes of aerosol at the ground. This leads to 0.667 ppmw of "observed aerosol" (model 1) or 42 ppbw of EC, the most significant component. In the cases with uncontaminated "basic aerosol" (model 3), after removal of EC and sulphuric acid, the aerosol material in the snow is reduced to 0.465 ppmw. Snow grains have a radius of 200 μm.

In haze as well as in no-haze cases the aerosol optical depth at 0.55 μm increases by approximately 120% mainly due to the contamination by sulphuric acid (24% by mass). This large response is due to the hygroscopic properties of sulphuric acid which greatly enhances the visual appearance of the haze.

4.1.1. No-haze condition. In the no-haze situation (A0 to A3) the aerosol causes warming in thermal and solar regimes at the top and at the ground level except at the surface in the case A2 with pure snow. The latter is analogous to the results of Shaw and Stamnes (1981), Porch and MacCracken (1982) and Cess (1984) who also found warming of the atmosphere and cooling of

Table 3. *Radiation balance ($W \cdot m^{-2}$), planetary (LPA) and surface albedo (A in %) for various cases*

Case	Optical depth	Top (10 mb)		Surface		Atmosphere		LPA	A
		Thermal	Solar	Thermal	Solar	Thermal	Solar		
A0	0.0	−169.46	100.57	−44.78	53.39	−124.68	47.14	66.15	78.11
A1	0.081	−169.36	108.33	−44.40	54.20	−124.96	54.13	63.54	76.79
A2	0.081	−169.36	106.70	−44.40	52.47	−124.96	54.23	64.09	77.56
A3	0.038	−169.39	102.16	−44.64	53.53	−124.75	48.63	65.62	77.71
B0	0.0	−169.62	101.33	−44.65	52.64	−124.97	48.69	65.89	78.31
B1	0.388	−170.36	108.43	−44.30	52.41	−126.06	56.02	63.51	76.46
B2	0.388	−170.36	106.82	−44.30	50.69	−126.06	56.13	64.05	77.27
B3	0.170	−170.32	102.44	−45.02	52.34	−125.30	50.10	65.52	77.65

(A) represent the no-haze conditions while (B) is the haze conditions. Sub-indices represent: (0) no-aerosol, (1) anthropogenic aerosol in the atmosphere and snow, (2) pure snow and (3) "basic aerosol" in the atmosphere and snow. Further details are given in Table 4.

Table 4. *Description of various cases investigated in Tables 1 and 3*

Cases	Experiment
	Realistic conditions. Spring temperature, aerosol scale height = 1.5 km, low level of snow contamination (effective savenging ratio of 1.02×10^5). Variable haze thickness and density. Solar declination for April 15. 10 snow layers of 1 cm of equivalent liquid water. Radius of ice grain is 200 μm.
A0	Low relative humidity (no haze); no aerosol
A1	As A0 but aerosol model 1 (observed aerosol) in air and snow layers
A2	As A1 but no aerosol material in snow (i.e. pure ice)
A3	As A0 but aerosol model 3 (natural aerosol) in air and snow layers
B0	Average haze condition: 99.5% humidity and 0.3 km thick; no aerosol
B1	Haze episode. As B0 but aerosol model 1 in air and snow
B2	As B1 but no aerosol material in snow (i.e. pure ice)
B3	Uncontaminated haze. As B0 but aerosol model 3 in air and snow

the surface. The cooling trend at the surface is due to depletion of the incident flux. However the expected contamination of the snow reduces the snow albedo sufficiently to reverse the trend. Instead of a small cooling of about 1 W m^{-2}, the surface is warmed by a similar amount.

Examining the change in surface albedo from A0 to A2 to A1, it is seen that the reduction of the albedo is not only due to an increase of snow contamination by absorbing material but also to a direct to diffuse conversion of the incident solar flux. Between A0 and A2, the increase in atmospheric scattering depletes the direct solar beam to the benefit of the diffused component (shown in the next section). Further, the albedo for diffused radiation is lower than the albedo for the direct beam if the solar zenith angle is larger than about 50° (Wiscombe and Warren, 1980). The effect of flux conversion from direct to diffuse components reduces significantly the albedo by 0.55 while the snow contamination by aerosol material reduces the albedo by an additional 0.77.

The planetary albedo approximately follows the surface albedo and is about 12% lower in absolute value, indicating substantial absorption within the atmosphere. This aerosol is responsible for an absorption of 7 W m^{-2} (A1–A0) and a total earth-atmosphere daily averaged warming of 7.8 W m^{-2}.

A weak but interesting effect is the coupling between surface albedo and atmospheric absorption. When the surface albedo is reduced the atmospheric absorption also decreases since the reflected radiation and the absorption of the return flux are reduced. This interaction affects mostly the region immediately above the surface. For a change of 0.77% in the albedo (A2–A1) the atmospheric warming is reduced by 0.1 W m^{-2}.

The thermal regime exhibits a normal "greenhouse effect". With increasing aerosol optical depth (A0 to A3 to A1) the net upwelling infrared at the top decreases by 0.1 W m^{-2} while the net surface infrared also decreases (0.4 W m^{-2}) due to the strengthening of the downward atmospheric counter radiation. The net result is a weak cooling of the atmosphere (0.3 W m^{-2}).

Although in the above cases (A0 to A3) some of the effects were small, they were mentioned because the conditions under which some of these mechanisms become important should be explored. In the next section, the effect of haze is examined. In the present model, a haze episode is simulated by increasing relative humidity close to saturation relative humidity. Although those conditions agree with observations by Mendonca et al. (1981), at least part of the haze is expected to be ice crystal nucleated at a relative humidity near or above 80% relative humidity depending on the temperature.

4.1.2. Haze condition. The typical haze is represented by a relative humidity of 99.5% in a 0.3 km layer adjacent to the surface (curve 4 Fig. 4b and case B0 to B3). From the no-haze situation (A0 to A3) the optical depth consistently increases by almost a factor 5. The net radiation at the top indicates a small cooling of the earth-atmosphere system in the thermal and only a modest increase of the total solar warming. It is of interest to note the change of sign in the thermal trend. In a sense, the "greenhouse effect" now shows an "abnormal" behaviour, that is an increase in the vertical confinement of the aerosol optical thickness in the haze layer, associated to the temperature inversion, results in an increase of the upward component of the infrared radiation. Comparing the change in net thermal radiation at the top between cases B0, B3 and B1, it is evident that the enhanced cooling is due to the "basic haze" component (B3–B0) and that sulphuric acid (B1–B3) adds only a small effect despite the considerable increase in optical depth (0.17 to 0.39). This will be further examined in the next section where interactions with surrounding drier aerosol are studied.

In the solar regime, considering the sulphuric acid-EC coupling (Blanchet and List, 1983) which can double the absorption coefficient from dry to wet aerosol, it is somewhat surprising to find a decrease in the total absorption when the relative humidity is raised. Effectively, while the gaseous absorption increases by 0.8W m^{-2} (B0–A0), the aerosol absorption decreases from 7.8 to 7.1 W m^{-2} (A1–A0 to B1–B0). The increase in back scattering due to considerable particulate growth overcompensates for the increase in aerosol absorptivity between no-haze and haze. This effect shows that scattering properties of the haze have a significant impact on the energetics despite the high surface reflectivity. This result agrees qualitatively with that obtained by Cess (1984) on compensating effects between scattering and absorption. But a word of caution is appropriate. By neglecting scattering an error of the order of 10% is introduced in the results. However, if the sulphuric acid-EC coupling is considered, neglecting scattering will result in an overestimation of absorption by about a factor 2.

If we further decompose the above result into basic and anthropogenic components, it is seen again that most of the depletion due to scattering is generated by the "basic haze" components; i.e. a change of 1.6 to 1.1 W m^{-2} (A3–A0 to B3–B0) in the "basic aerosol" as opposed to a change of 6.2 to 6.0 W m^{-2} (A1–A3 to B1–B3) in the anthropogenic components. Assuming that the aerosol composition does not change substantially between a haze and a no haze situation, the above result implies a net cooling in the thermal and solar ranges due to the haze episode. In other words, the solar warming effect is stronger in drier atmosphere. However, the anthropogenic components by themselves have a pronounced warming effect with respect to the "basic aerosol"; i.e., a factor 3.9 (A1–A3)/(A3–A0) for no-haze increasing to 5.5 (B1–B3)/(B3–B0) in the haze case. This 40% increase is caused by the internal mixture sulphuric acid and EC.

The surface budget for the average haze indicates a reduction of the net solar radiation but again a considerable recovery from direct to diffuse conversion and snow contamination. Here it is noticeable from the surface albedo change that this effect is doubled in strength, from 0.55% in the dry case (A2–A0) to 1.04% in absolute value for the haze case (B2–B0). However the recovery is not as strong as in the dry case (+0.8 W m^{-2} (A1–A0)) due to attenuation from back scattering. The result is a cooling of the surface (−0.2 W m^{-2} (B1–B0)) rather than a warming.

The atmospheric radiation budget for the average haze shows an increase in the thermal cooling due to anthropogenic contamination (0.8 W m^{-2} (B1–B3)) which was not apparent from the net thermal radiation at the top. This implies that most of the exchange takes place between the atmosphere and the surface, and that the anthropogenic aerosol is not significantly changing the amount of energy lost to space. The solar absorption by the atmosphere increases (7.0 (A1–A0) to 7.3 W m^{-2} (B1–B0)) due to the haze condition. Therefore, the net cooling of the column atmosphere-ground is essentially due to the decrease of absorption at the surface from attenuation due to back-scattering of the incident radiation across the hazy atmospheric layers.

Finally, in the extreme haze situation, when the relative humidity is increased to 99.9% and the haze layer is 1 km thick (curve 5 Fig. 4b), all the above results are enhanced. The effect of diffuse to direct conversion of the solar irradiance is tripled with respect to the no haze condition and depletes the surface albedo by as much as 1.5%. The infrared is particularly sensitive to the increase in size distribution of the particles. This leads to an important question which should be addressed in future studies. Highly diluted sulphuric acid droplets would eventually crystallize and grow to precipitation size. Those particles with much lower specific density than water have an increased geometric size and a larger cross-section for scattering of solar radiation and emission of thermal radiation. It is therefore important to determine the phase of Arctic haze particles.

4.2. *Vertical and spectral structure of the radiation perturbations*

In this experiment the consequences of a steep thermal inversion typical of the winter Arctic haze are examined and interactions between adjacent dry and moist layers of aerosol are considered. To estimate the potential magnitude of perturbations of the radiation balance is of interest to climate studies. The nature and strength of the perturbation signal is also determinant for future time dependent investigations. In the present experiment however, the conditions are not set to represent a particular time of the year, but rather to represent situations that are instructive on the behaviour of the radiation field in haze.

The winter atmosphere (Fig. 4) is represented with the aerosol vertical distribution as observed by Rahn (solid line in Fig. 4c). It is characterized by a haze layer in the lowest kilometre and a pronounced dry aerosol layer between 2 and 5 km. The haze condition is simulated by increasing the relative humidity to 99% in a layer between 0.13 and 0.54 km above the ground. Since the snow surface has a high contamination at the end of the melting period, the concentration of EC is set to 1.2 ppmw, uniformly mixed in the snow layers. As seen below, only the EC in the top most snow layer (1 cm of ELW) significantly affects the albedo. The amount of EC in that surface layer is comparable to the total amount in the atmospheric column.

The effect of aerosol on radiative transfer in the atmosphere is generally a function of chemical composition, relative humidity of the air, size distribution of particles and wavelength. Furthermore spectral fluxes are dependent upon air temperature, amount of absorbers and surface reflectivity. All these physical quantities are variable in the present model. In the following, the effect of the aerosol perturbation on spectral fluxes at the top of the model, on the vertical profiles of the fluxes and on the heating rates are examined successively.

4.2.1. Spectral irradiance perturbations at the top of the model. Line (1) in Fig. 5 shows the incident solar spectral flux at the top of the atmosphere. The dotted line (2) represents the diffuse upwelling irradiance from scattering by air molecules, aerosol particles and the snow surface. Molecular scattering dominates in the ozone window near 0.4 μm but beyond that point the upward flux is progressively controlled by the surface reflectivity as one can see by departure from the inverse fourth power of wavelength. The sharp dip near 1.3 μm is due to strong absorption by snow grains in the infrared. Between 3 and 7 μm is the region where solar and terrestrial radiation significantly overlap. Most of the upward thermal radiation comes from the 7 to 30 μm region. In Fig. 5 the thicker line (3) is the total downward irradiance incident on the surface. High atmospheric transmission between the water absorption band in the near infrared,

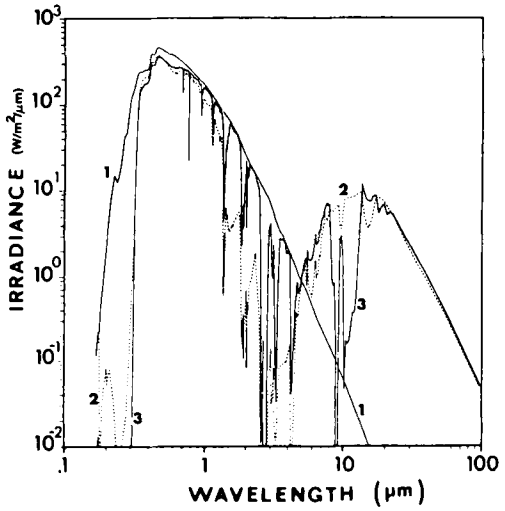

Fig. 5. Spectral irradiance generated by the radiation model. The thinner solid line (1) represents the incident solar irradiance, the dashed line (2) is the total flux scattered or emitted to space while the thicker solid line (3) is the total flux received at the surface. In the actual study, departures of these spectra due to the introduction of various aerosol components are investigated.

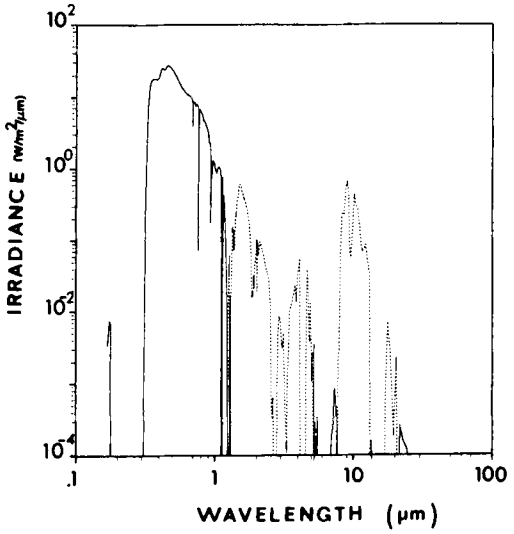

Fig. 6. Spectral irradiance perturbation of outgoing radiation at the top of the atmosphere due to "basic haze" (model 3, i.e., without sulphuric acid nor EC) in moist conditions. Solid line represents a decrease (or warming) and dashed line represents an increase (or cooling).

together with lowering of the snow surface albedo makes this region an efficient heat source for the surface. In the thermal regime, regions 14 to 30 μm and near 7 μm are also important source terms for the surface. On the other hand the deep window region is the principal radiative sink of the surface energy balance. In the following the departure of the upward irradiance lost to space and attributed to various components of the aerosol is examined.

Fig. 6 shows the resulting change in the upward diffuse flux at the top of the atmosphere between "basic haze" and situations without aerosol. Most dips in the curve correspond to gaseous absorption bands. The "basic haze" produces a genuine gain of energy at wavelengths smaller than 1.3 μm where a sharp cutoff in the surface albedo occurs. Above that threshold the upwelling flux is increased by the aerosol layer. In the longwave region, the dominant contribution comes from the 7.8 to 13 μm window region with secondary peaks around 4.9 and 19 μm where the transmittance of water vapour is relatively high. The reduction by up to one order of magnitude in upward flux around 9.6 μm indicates an effective transfer of radiative energy between the haze layer and the ozone layer in the stratosphere. The narrow water vapour window at 3.3 to 4.2 μm may be dominated by solar or thermal radiation depending on the solar zenith angle.

Fig. 7 shows the corresponding result for a drier atmosphere where the relative humidity does not exceed 50% (no-haze case). Below 1.3 μm, the lowering of the relative humidity results in a substantial increase of absorption due to reduction in the back-scattered fraction. Differences become increasingly large above 1.3 μm, due to the sensitivity of the infrared radiation to droplet size. The most striking change takes place in the windows where the amplitude decreases by more than one order of magnitude. In this situation the aerosol exhibits a normal "greenhouse effect". The increase of humidity accompanying the haze episodes is a cooling factor in the aerosol perturbation both in solar and thermal regimes. In the winter without solar radiation the haze is a cooling agent through the 8 to 12 μm window.

Fig. 8 represents the contribution due to anthropogenic components alone on top of the "basic aerosol" component. Soot greatly increases the absorption in the visible as indicated by the

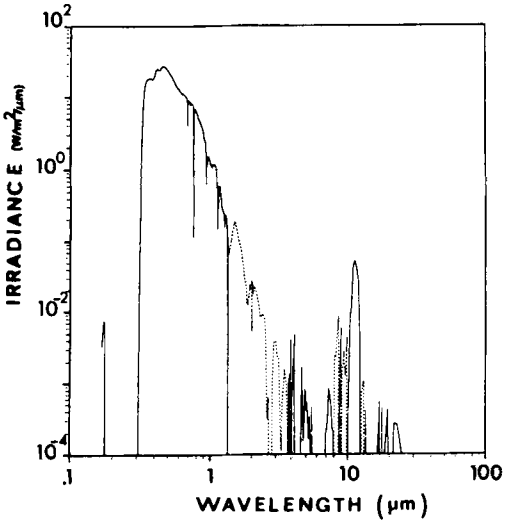

Fig. 7. As Fig. 6 but for drier atmosphere (no-haze conditions, model 3).

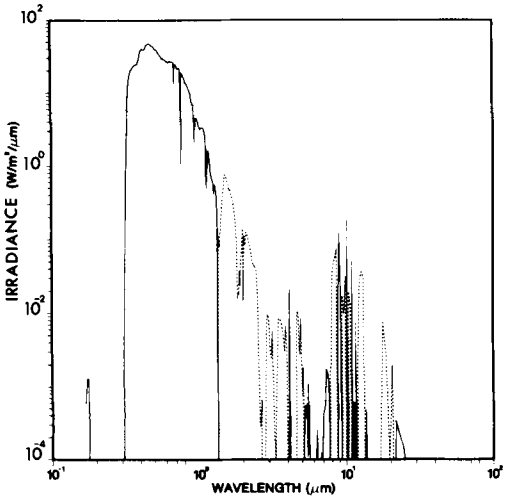

Fig. 8. As Fig. 6 but for anthropogenic perturbation during haze episodes (sulphuric acid and EC only, model 1—model 3).

marked depletion in the reflected radiation (higher values reached by the solid line), while only small increases of upwelling flux are noticeable above 1.3 μm. A good portion of the increased absorption in the visible is due to the EC component in the snow layer which lowers the surface albedo. In the window the rapid change of sign is associated with the variation of the imaginary index of sulphuric acid and weak absorption by water vapour and ozone. Again this shows that the sulphuric acid, which is mostly responsible for the haze opacity at all wavelengths, results in remarkably weak net effects on the upwelling thermal irradiance at the top of the atmosphere. This aspect remains to be explained.

Overall, the above diagnositics stress that the dominant contribution of the anthropogenic substance occurs in the visible part of the spectrum with a warming effect. A weak cooling trend dominates above 1.3 μm. The "basic haze" has a longwave cooling action particularly significant during winter time. The anthropogenic component has an erratic behaviour in the 8 to 12 μm window and adds very little net energy to the upwelling radiation at the top of the atmosphere. Segregation between the effect of EC and sulphuric acid indicates that the latter is responsible for that behaviour. Soot has a systematic cooling effect throughout the entire window and, despite its low concentration, dominates the overall perturbation in that spectral region.

4.2.2. Vertical profiles of solar irradiance perturbations. The vertical profiles of solar irradiance perturbations (downward direct, diffuse, total, upward diffuse and the net fluxes) for the present case are now examined. The effect of EC (model 2–model 3) and sulphuric acid (model 1–model 2) are analyzed individually (Fig. 9a and 9b). The negative scale at the bottom of those figures represents the snow depth in units of 5 cm of ELW.

Sulphuric acid (Fig. 9a) produces strong scattering and weak absorption. The conversion direct to diffuse is dominant and the change in total downward irradiance is small. This is essentially the behaviour observed by Mendonca et al. (1981). In the center of the dry aerosol layer (3 km) the direct solar beam is depleted by 7 W m^{-2} essentially to the benefit of the diffuse component. The weaker direct solar beam is further depleted (by 13 W m^{-2}) when crossing the haze layer above the surface. The change in total downward flux (line 3) is due to back-scattering and absorption. The flux convergence of 2 to 3 W m^{-2} is due to the sulphuric acid-EC internal mixture. Sulphuric acid alone has negligible absorptivity in the visible. The absorption shown here is due to enhanced absorption by the EC

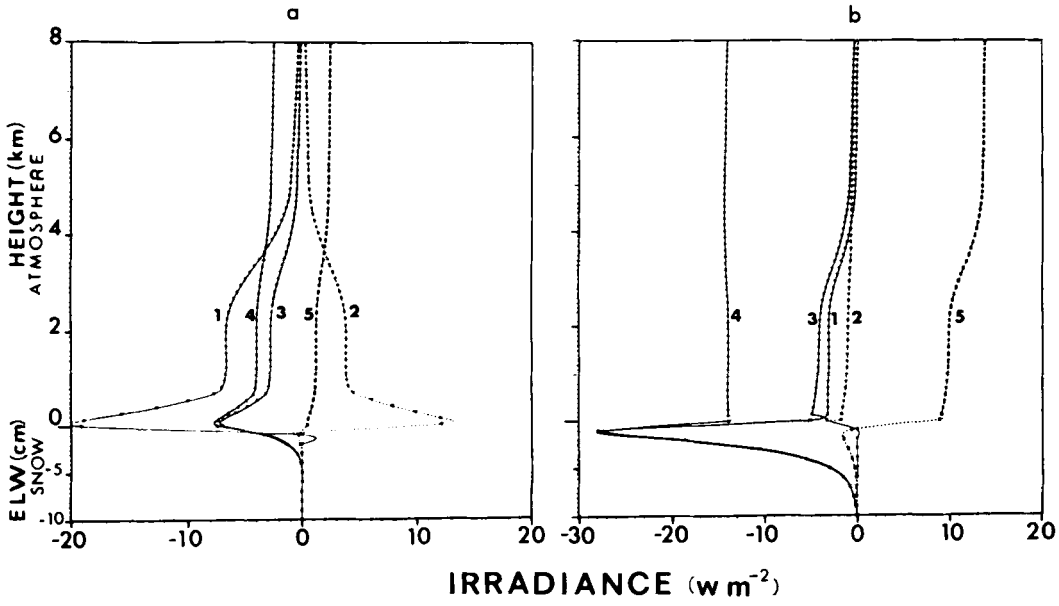

Fig. 9. Vertical profiles of the solar flux components. Curves are for direct beam (1), diffuse downward flux (2), total downward flux (3), diffuse upward flux (4) and net flux (5). Heights in the atmosphere (>0) are in units of kilometers while they are in units of 5 cm of equivalent liquid water (ELW) in the snow (<0). (a) Perturbation due to sulphuric acid and its interaction with EC as an internal mixture (model 1–model 2). (b) Perturbation due to EC alone (model 3—model 2).

kernel (within the aerosol particles) from the presence of a sulphuric acid coating shell. Above the surface, the upward diffuse flux is less perturbed than the downward flux, the absorption being compensated by back scattering from the downward components. This illustrates clearly the counter action between absorption and scattering. The variation of the net flux convergence takes place mostly in the dryer aerosol layer between 1 and 4 km.

The change in profiles of solar irradiances attributable to the addition of EC on top of the "basic haze" (aerosol model 3) is shown in Fig. 9b. As opposed to sulphuric acid, the conversion direct to diffuse is very small and absorption dominates. Consequently all flux components are depleted. Most of the flux convergence is in the dry layer. In snow, at such a high concentration, EC leads to a flux convergence of about 10 W m^{-2} at the surface and cooling of about 2 W m^{-2} below 1 cm of ELW. This shows that only EC located in the surface snow layer has a significant effect on the albedo.

4.2.3. Vertical profiles of thermal irradiance perturbations. The presence of the thermal inversion results in an increase of upward thermal irradiance from the surface to the top of the inversion (2 km). Under clear skies the snow surface emits through the window nearly like a black body and due to the low thermal conductivity of snow and modest eddy diffusivity from the atmosphere to the surface in the stably stratified air, a relatively low temperature equilibrium is reached at the surface. This situation limits the radiative cooling of the system. However, if a grey body such as a cloud or a haze layer is placed in the inversion layer the emission temperature increases with height and can increase considerably the cooling to space occurring in the windows. From this point of view the energy balance of the Arctic can be seriously altered by changes in the cloud cover or haze optical thickness.

The vertical profiles of thermal irradiance perturbations for a cloud and the present haze case (Fig. 6) are examined. First, the case of a

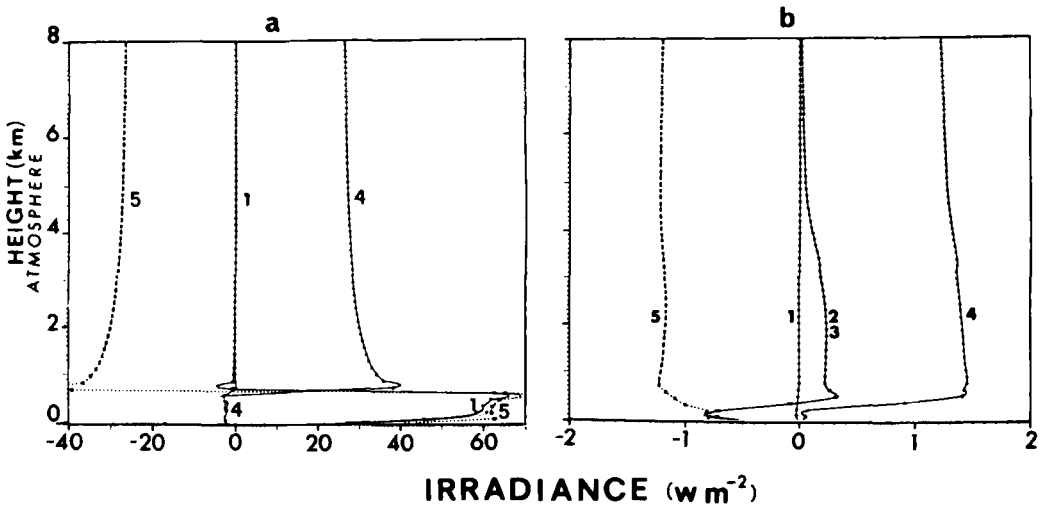

Fig. 10. Vertical profiles of the thermal flux components. Curves are for direct solar beam above 3 μm (1), diffuse downward flux (2), total downward flux (3), diffuse upward flux (4) and net flux (5). (a) Perturbation due to a stratus cloud with a constant optical depth of 10. (b) Perturbation due to "basic haze" (model 3–no aerosol) without EC nor sulphuric acid.

stratus layer is illustrated in Fig. 10a. Here the cloud has an optical depth of 10 at all wavelengths and occupies a single model layer between 912 and 930 mb. The single scattering albedo is assumed constant at 0.4 throughout the infrared spectrum. A sharp discontinuity in the downward flux is seen below the cloud. This flux increases by more than 60 W m^{-2} and most of this energy reaches the surface. A little more than 2 W m^{-2} from the direct solar beam above 3 μm is absorbed by the cloud layer. The upward flux sharply increases by 40 W m^{-2} at the top of the cloud with substantial attenuation in the first 2 km above the cloud. The net flux profile shows a very large divergence within the thin cloud layer. This strong energy depletion, directed toward the ground and the upper atmosphere, is partly reabsorbed by the atmosphere in the adjacent 1 or 2 km around the cloud. The most significant effect from the point of view of the system's energy is the increase of about 25 W m^{-2} in the flux lost to space. In such a case, one would expect considerable turbulent transport around the cloud boundaries leading to eventual modification of the temperature profile and radiative fluxes. The cloud favours energy exchange within the atmosphere and constitutes an efficient mechanism for depletion of internal energy by genuine increases in the thermal radiation lost to space.

The change in thermal fluxes due to the addition of the "basic haze" (model 3) is shown in Fig. 10b. The downward diffuse flux increases with particulate concentration in the dry aerosol layer (r.h. near 20%). At the top of the moist layer (r.h. = 99% at 0.6 km of altitude) the downward flux increases but in the bottom half of the haze layer the absorption of downward flux dominates over the emission and the resulting flux received by the ground is reduced by 0.8 W m^{-2} with respect to the case without aerosol. The upward flux increases sharply in the moist layer up to 1.5 W m^{-2} at the top of that layer due to increased temperature and optical depth in the 10 μm window. Above 1 km the upward flux is depleted by atmospheric absorption. The net flux is increased by 1.2 W m^{-2} almost constant with height and is directed upward. This pattern is similar to that produced by a stratus cloud (Fig. 10a), however, the amplitude is more than one order of magnitude smaller. The "basic haze" increases the radiative cooling efficiency of the atmosphere by less than 1% while the thin stratus cloud increases the cooling in the column by 17%. But unlike the cloud, the basic haze can actually cool the surface as seen from the decrease of

about 1 W m^{-2} in the downward flux at the surface. This peculiarity is due to more absorption of the incident flux from above the haze layer (0.6 km) than to downward emission from the lower half of the layer (i.e. an inverse "greenhouse effect"). In other words the "basic haze" has a masking effect on the temperature inversion as seen from the ground.

The results of the anthropogenic perturbations (sulphuric acid and EC) on top of the "basic haze" (Fig. 10b) are illustrated in Fig. 11a and 11b for sulphuric acid and EC, respectively. Soot in the thermal regime has a similar behaviour to the "basic haze" but is one order of magnitude weaker. With an amplitude of about 0.1 W m^{-2} this perturbation is negligible in comparison to other effects. Fig. 10a shows the change (model 1 – model 2) in irradiances due to the coating of the aerosol by sulphuric acid. Despite the relatively substantial amount of sulphuric acid and its strong hygroscopic properties, its impact on the flux profile is modest. Furthermore its behaviour is very different from that of the "basic aerosol", EC component or the cloud; the increase in the net upwelling thermal irradiance is small, even smaller than that of the minute amount of EC and the increase in downward flux is larger and positive at the surface. The reason of this result is the hygroscopicity of sulphuric acid. Because the acid droplets grow considerably in dry air (10 to 30%), the opacity of the haze increases significantly at all relative humidities. As a consequence the internal exchange between atmospheric layers is enhanced with respect to the loss to space characteristic of a sharp transition such as a cloud top. The net result, in contrast to that of the "basic haze", is virtually no change in the thermal cooling of the earth-atmosphere system, but a slight cooling of the atmosphere to the benefit of the surface. On the other hand, deliquescent aerosol particles exhibit a sharp increase in the emissivity at their deliquescent point (r.h. near 80%) and produce a definite haze top similar to that of a cloud. In a very stable atmospheric profile, it is the "degree of vertical confinement" of the aerosol layer that determines the net thermal energy lost by the atmosphere to space. This confinement is optimum in a thin stratus layer and larger for deliquescent aerosols than for hygroscopic aerosols. The effect becomes

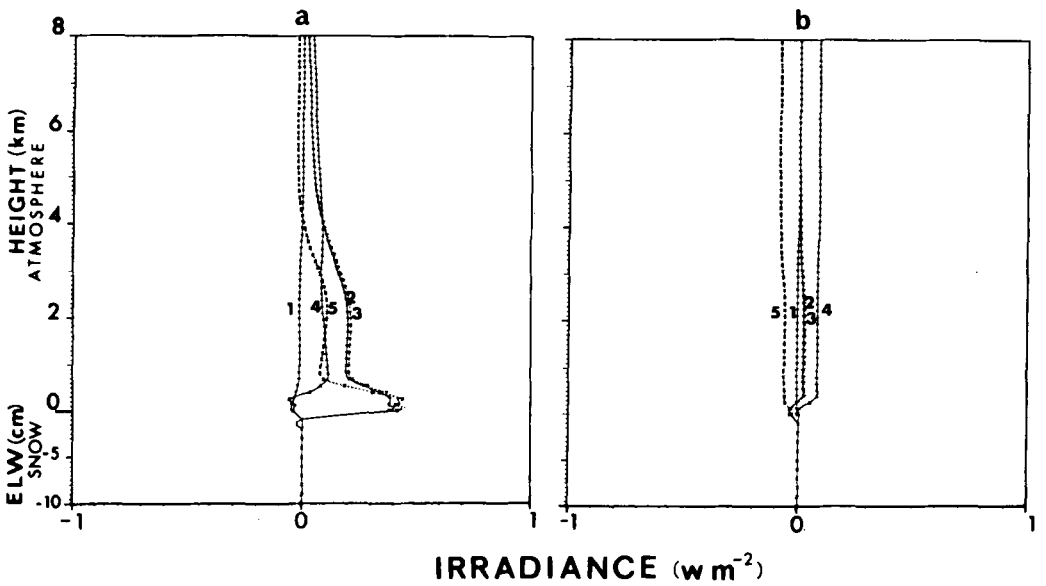

Fig. 11. As Fig. 10 but for (a) sulphuric acid (model 1—model 2) and (b) for EC components only (model 2—model 3).

more evident when the flux divergence is considered.

4.2.4. Radiative heating rates. It is convenient to examine the convergence of the radiative fluxes in the form of heating rates (°K/day). This quantity is of interest for the energetics of the atmosphere and is often used in climate modelling and its diagnostics. The results are essentially similar to the above but give a better perspective of the amplitude of each term. The total radiative heating rates for the solar and thermal regime in the haze case are shown in Fig. 12a. During mid-April the daily mean solar heating rate is much weaker than the thermal cooling rate. The thermal cooling is characterized by rapid variation due to absorber amount and temperature profile. The dashed line represents the total daily average heating rate which is dominated by thermal radiation.

The temperature inversion leads to considerable heating near the surface due to strengthening of the downward flux convergence. This appears to be one reason for the observed extensive haze formation in the Arctic atmosphere during spring. As relative humidity increases in the boundary layer form downward eddy heat flux over the radiatively cooled surface, the highly hygroscopic sulphate aerosol absorbs water and increases its particulate volume several hundred fold. This increase in opacity enhances the absorption of downward radiation near the surface (Fig. 12b and 10b) and inhibits the activation of aerosol particles to form cloud droplets. The result is a relatively stable haze layer at a relative humidity just under saturation. This also inhibits the preciptation process and results in long residence times characteristic of the Arctic aerosol particles during winter and spring.

The perturbation heating rate due to the EC component alone is shown in Fig. 13b. The most prominent feature is the solar heating in the dry aerosol layer. Absorption in the haze layer (below 1 km) is attenuated due to attenuation of the downward irradiance through the elevated dry layer and large mean air mass. There is no significant change due to EC in the thermal regime. The effect of sulphuric acid is seen in Fig. 13a. The solar heating is mostly due to a

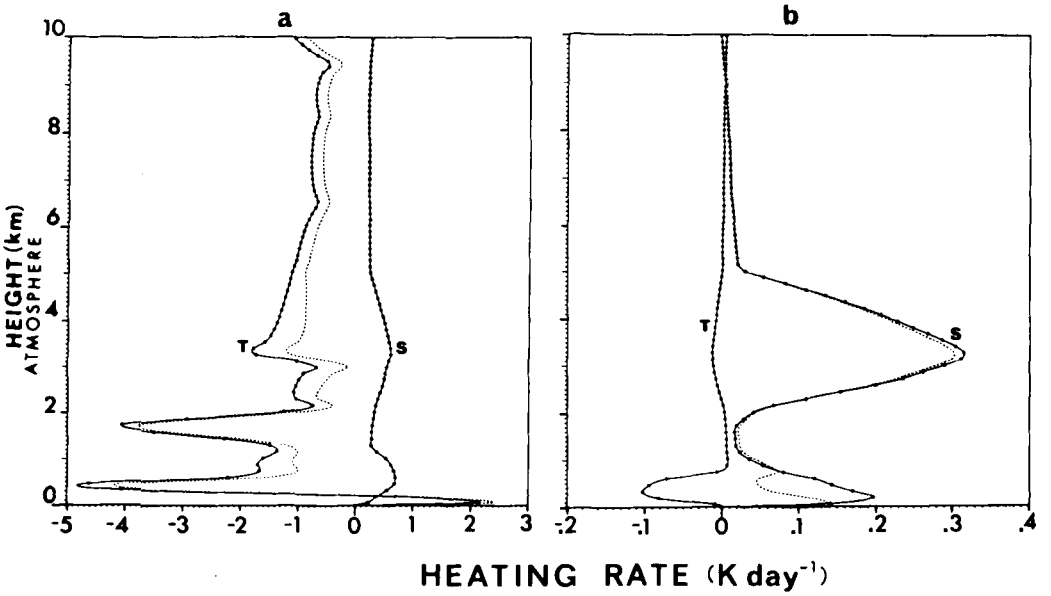

Fig. 12. (a) Radiative heating rate profiles due to atmospheric gases (winter atmosphere of Fig. 4) and aerosols. Solar (S) and thermal (T) terms are shown together with the net heating rate (dashed line). (b) Perturbation of the raditive heating rate due to all aerosol components (haze below 1 km and dryer aerosol around 3 km).

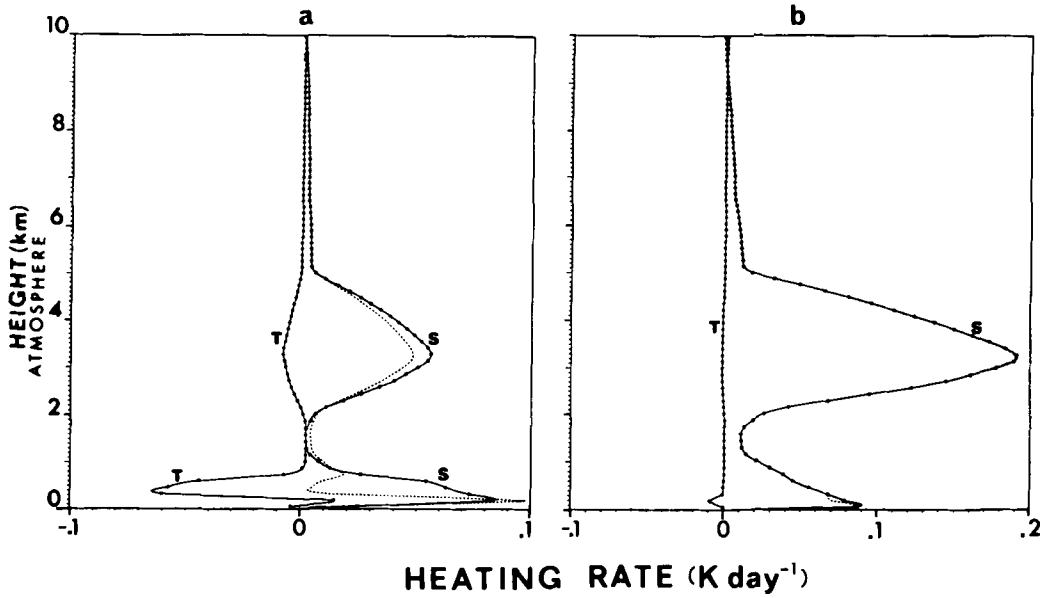

Fig. 13. Radiative heating rate perturbation profiles (a) due to sulphuric acid and its interaction as an internal mixture with EC (model 1—model 2) and (b) due to EC component only (model 2—model 3). Solar (S) and thermal (T) terms are shown together with the net heating rate (dashed line).

coupling effect from the internal mixture with EC and represents a significant contribution. Thermal cooling nearly offsets the solar warming in the top part of the haze layer. The slight cooling in the dry layer is enhanced by the hygroscopic properties of sulphuric acid. The effect of the total aerosol ("basic" + anthropogenic) shown in Fig. 12b demonstrates that the solar heating rate is mostly affected by the anthropogenic part and the thermal cooling rate is equally affected by "basic" and anthropogenic components.

Recently, Rosen and Hansen (1984) reported the first direct measurements of vertical profiles of graphitic carbon (EC) concentration. From the measurement of the mass concentration of carbon and using aerosol models they estimate the vertical absorption coefficient profile of a few particular cases of interest. Fig. 14 shows the daily mean solar heating rate evaluated using the present radiation model together with their absorption coefficient profile (March 31, 1983 at 74°N 25°E, their Fig. 3). The atmospheric conditions are set to the sub-Arctic standard

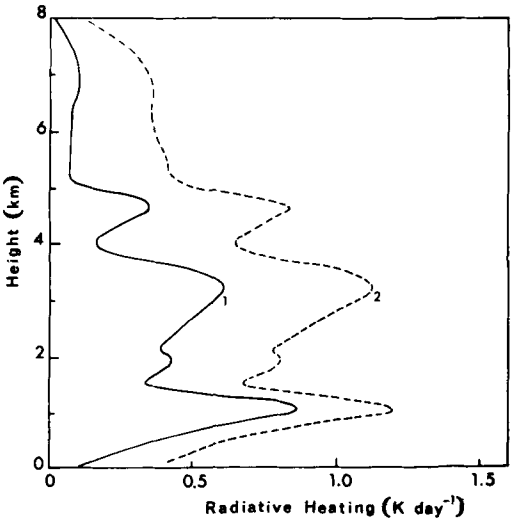

Fig. 14. Daily mean solar heating rate computed for the vertical extinction profile obtained by Rosen and Hansen (1984) on March 31, 1983 at 74°N 25°E. Curve 1 represents the aerosol contribution only while curve 2 also contains the heating rate for gases in a sub-Arctic standard atmosphere (McClatchey et al., 1972).

atmosphere (McClatchey et al., 1972). The heating rate for the aerosol is comparable to that from gaseous absorption and the multi-layer structure is reflected on the flux convergence. The effect of EC is more than 3 times larger than that obtained in the case shown in Fig. 12b. Fig. 14 might represent a rather extreme situation of the radiative heating due to Arctic aerosol. On the other hand, the plate transmission method used by Rosen et al. tends to overestimate the absorption coefficient by a factor 2.5 with respect to the integrating plate method (Sadler et al., 1981). Another source of differences is the aerosol model. Rosen and Hansen assumed a log-normal distribution with a mean mode radius of 0.2 μm and a standard deviation of 2 obtained from Whitby (1978) for the urban aerosol. Furthermore they used a complex refractive index of $1.94 - 0.66i$ which is representative of pure graphite. The Arctic aerosol is characterized by a narrower distribution of smaller particles (Heintzenberg, 1980). Blanchet and List (1983) used a main accumulation mode radius of 0.087 μm and a narrower size distribution (the width $\sigma = 1.4$ for the main accumulation mode) together with lower spectral refractive index ($1.74 - 0.44i$ at 0.55 μm) to represent impure and loosely aggregated carbon chains. The result is evident when comparing the specific absorption of both aerosol models. Rosen and Hansen obtain a specific absorption of 18.1 m^2 per gram of EC (their model 1) as compared to 5.0 m^2 per gram of EC for the model used in the present study (our model 1, dry case). Therefore the differences found in the heating rates are likely to originate in the usage of different assumptions for the aerosol models. More observations are needed in order to determine precisely the specific absorption of the Arctic aerosol.

5. Summary

In this study, a column radiation model is developed to incorporate the most important processes which determine the radiation budget. The well established delta-Eddington method is extended to treat the thermal radiation by adding the source term in the radiative transfer equation. Complete overlap between solar and thermal region is kept. Instead of the usual sum of exponential fits, a different approach is used to calculate the transmission; the optical depth is evaluated from a band model which can account for a large number of gases, provides a better temperature dependence and allows higher spectral resolution for comparable computer time. In the visible and in the near infrared the model calculates the snow surface albedo from Mie parameters of ice grains and optical parameters of aerosol models. Thus, both the anthropogenic pollution of the aerosol and of the snow surface are considered. Therefore this model allows the investigation of the effects of the Arctic haze and of the anthropogenic pollution on the energy balance of the atmosphere and of the earth's surface.

In the solar domain, the results demonstrate that the presence of sulphuric acid approximately doubles the optical depth of the haze while the internal mixture of sulphuric acid with graphitic material can increase the solar absorption by about 40%. On the other hand, at relative humidities near saturation, the increase of backscattering reduces the absorption in the boundary layer and compensates for the increase due to the internal mixture. The total absorption of the anthropogenic aerosol is estimated to be 4 to 5 times the absorption by the "basic aerosol". For mid spring conditions the solar heating of the system is found to be lower by a factor 2 to 3 than earlier estimates (20 to 30 $W \cdot m^{-2}$). The main reasons for that difference being the lower optical depth for absorption and the daily average insolation. Further it is shown that the previously expected cooling at the surface can be offset by a change in surface albedo from conversion of the direct solar beam to a diffuse component during haze episodes and from a contamination of the snow surface by EC material in amount of the order of 50 PPBW. The scattering properties of the aerosol during haze episodes considerably attenuates that atmospheric warming by depleting the incident solar flux due to enhanced back scattering.

In the thermal radiation domain, low level stratus cloud located in a region warmer than the surface can dramatically increase the exchange of radiative energy with the surface and surrounding atmosphere but, more significantly, enhance the net loss of energy to space by 10% to 20%. In the case of Arctic haze, the increase in upwelling flux is qualitatively similar to the effect of a

stratus cloud embedded in a warm layer but it is more than one order of magnitude weaker. Even in strong winter temperature inversions the increase in thermal flux is found to remain below 1% of the total thermal radiative energy lost to space. Nevertheless, this perturbation is comparable to that of doubling carbon dioxide but opposite in sign. Thus even during winter, large scale haze is expected to have a significant effect on the energy balance of the Arctic. This earth-atmosphere column cooling is essentially caused by deliquescent compounds in the aerosol. Hygroscopic but non-deliquescent materials like sulphuric acid in the wet aerosol result in internal exchange of radiant energy but no significant loss to space. The cooling rates become comparable to the solar heating rate only in haze layers. In dry atmosphere the contribution of the aerosol to the thermal cooling rate may be neglected.

6. Acknowledgement

This research was sponsored by the Atmospheric Environment Service of Canada. Part of the work was done while one of the authors (J.-P.B.) was visiting the International Meteorological Institute in Stockholm, University of Stockholm and this author would like to acknowledge Dr. J. Heintzenberg, Dr. H.-C. Hansson and Dr. J. A. Ogren for many valuable discussions on the subject of the present work.

REFERENCES

Blanchet, J. P. and List, R. 1983. Estimation of optical properties of Arctic haze using a numerical model. *Atmos-Ocean 21*, 444–464.

Carlson, T. N. and Benjamin, S. G. 1980. Radiative heating rate for Sahara dust. *J. Atmos. Sci. 37*, 193–213.

Carlson, T. N. 1981. Speculations on the movement of polluted air to the Arctic. *Atmos. Environ. 15*, 1473–1477.

Cess, D. R. 1983. Arctic aerosols: model estimates of the interactive influences upon the surface-troposphere radiation budget. *Atmos. Environ. 17*, 2555–2564.

Cogley, A. C. and Borucki, W. 1976. Exponential appoximation for daily average solar heating or photolysis. *J. Atmos. Sci. 33*, 1347–1356.

Dave, J. V. 1972. Development of programs for computing characteristics of ultraviolet radiation. Technical report – Scalar case. NASA Technical Rept. NAS 5-21680, Greenbelt, MD.

Grassl, H. 1973. Influence of different absorbers in the window region on radiative cooling (and on surface temperature determination). *Beitr. Phys. Atmos. 47*, 1–13.

Hansen, J. E. 1969. Exact and approximate solutions for multiple scattering by cloudy and hazy planetary atmosphere. *J. Atmos. Sci. 26*, 478–487.

Heintzenberg, J. 1980. Particle size distribution and optical properties of Arctic haze. *Tellus 32*, 251–260.

Heintzenberg, J. 1981. The chemical composition of Arctic haze at Ny-Alesund, Spitsbergen. *Tellus 33*, 162–171.

Kneizys, F. X., Shettle, E. P., Gallery, W. O., Chetwynd, J. H., Jr., Abreu, L. W., Selby, J. E. A., Fenn, R. W. and McClatchey, R. A. 1980. Atmospheric transmittance/Radiance: Computer code LOTRAN 5. AFGL-TR-80-0067. Environmental Research Papers, No. 697. 233 pp.

Joseph, J. H., Wiscombe, W. J. and Weinman, J. A. 1976. The delta-Eddington approximation for radiative flux transfer. *J. Atmos. Sci. 33*, 2452–2459.

Lenoble, J. 1976. Review of radiative transfer methods in scattering atmospheres. *Inversion methods in the atmospheric remote soundings*. Ed. A. Deepak, Academic Press, 622 pp.

Luther, F. M. and Fouquart, Y. 1984. The intercomparison of radiation codes in climate models (ICRCCM) Longwave clear-sky calculations. Frascati, Italy, 15–18 August 1984. World Climate Programme. WCP-93, December 1984. 37 pp.

McClatchey, R. A., Fenn, R. W., Selby, J. E. A., Volz, F. E. and Garing, J. S. 1972. Optical properties of the atmosphere (3rd edition). ARCRL-72-0497. Environmental Research papers, No. 411. 108 pp.

Mendonca, B. G., DeLuisi, J. J. and Schroeder, J. A. 1981. Arctic haze and perturbations in the solar radiation fluxes at Barrow, Alaska. Proceeding from 4th Conference on Atmospheric Radiation. American Meteorological Society, Toronto, Ontario, Canada, June 1981, 95–96.

Porch, W. M. and MacCracken, M. C. 1982. Parametric study of the effects of Arctic soot on solar radiation. *Atmos. Environ. 16*, 1365–1371.

Patterson, E. M., Marshall, B. T. and Rahn, K. A. 1982. Radiative properties of the arctic aerosol. *Atmos. Environ. 16*, 2967–2977.

Rahn, K. A. 1978. Chemical and optical properties of the Barrow aerosol. Geophysical monitoring for climatic change, no. 7. Summary report for 1978. US Dept. of Commerce. 97–99. NTIS No. PB80-165962.

Rahn, K. A. and McCaffrey, R. J. 1979. On the origin and transport of the winter arctic aerosol. *Ann. New York Acad. Sci. 338*, 486–503.

Roberts, R. E., Selby, J. A. and Biberman, L. 1976. Infrared continuum absorption by atmospheric water vapor in the 8–12 μm window. *Appl. Opt. 15*, 2085–2090.

Rodgers, C. D. and Walshaw, C. D. 1966. The computation of infrared cooling rate in planetary atmospheres. *Q. J. R. Meteorol. Soc. 93*, 43–54.

Rosen, H., Navakov, T. and Bodhaine, B. A. 1981. Soot in the Arctic. *Atmos. Environ. 15*, 1371–1375.

Rosen, H. and Hansen, A. D. A. 1984. Role of combustion-generated carbon particles in the absorption of solar radiation in the Arctic haze. *Geophys. Res. Lett. 11*, 461–464.

Rothman, L. S. 1981. AFGL atmospheric absorption line parameters compilation: 1980 version. *Appl. Opt. 20*, 791–794.

Sadler, M., Charlson, R. J., Rosen, H. and Novakov, T. 1981. An intercomparison of the integrating plate and the LASER transmission methods for determination of aerosol absorption coefficients. *Atmos. Environ. 15*, 1265–1268.

Shaw, G. E. 1975. The vertical distribution of tropospheric aerosols at Barrow, Alaska. *Tellus 27*, 39–49.

Shaw, G. E. and Stamnes, K. 1980. Arctic haze: perturbation of the polar radiation budget. *Ann. New York Acad. Sci. 338*, 533–539.

Shettle, E. P. and Weinman, J. A. 1970. The transfer of irradiance through inhomogeneous turbid atmospheres evaluated by Eddington's approximation. *J. Atmos. Sci. 27*, 1048–1055.

Stone, H. M. and Manabe, S. 1968. Comparison among various numerical models designed for computating infrared cooling. *Mon. Wea. Rev. 96*, 735–741.

Thekaekara, M. P. 1974. Extraterrestrial solar spectrum, 3000–6000A at 1A intervals. *Appl. Opt. 13*, 518–522.

Valero, F. P. J., Ackerman, T. P. and Gore, W. J. Y. 1983. Radiative effects of the Arctic haze. *Geophys. Res. Lett. 10*, 1184–1187.

Warren, S. G. and Wiscombe, W. J. 1980. A model for the spectral albedo of snow. II. Snow containing atmospheric aerosols. *J. Atmos. Sci. 37*. 2734–2745.

Welch, R. M. and Zdunkoski, W. G. 1982. Back scattering approximations and their influence on Eddington-type solar flux calculations. *Beitr. Phys. Atmos. 55*, 28–42.

Wiscombe, W. J. 1973. Solar radiation calculations for Arctic summer stratus conditions. Climate of the Arctic. Edited by: G. Weller and S. A. Bowling. Proceedings from 24th Alaskan Science Conference. Fairbanks, Alaska, 15 to 17 August 1973, 245–254.

Wiscombe, W. J. 1977. The delta-Eddington approximation for a vertically inhomogeneous atmosphere. NCAR Technical Note TN-121+STR.

Wiscombe, W. J. and Joseph, J. H. 1977. The range of validity of the Eddington approximation. *Icarus 32*, 362–377.

Wiscombe, W. J. and Warren, S. G. 1980. A model for the spectral albedo of snow. I. Pure snow. *J. Atmos. Sci. 37*, 2712–2733.

Whitby, K. T. 1978. The physical characteristics of sulphure aerosols. *Atmos. Environ. 12*, 135–159.